

Superior piezoresistive strain sensing behaviors of carbon nanotubes in one-dimensional polymer fiber structure

Senlong Yu^a, Xingping Wang^a, Hengxue Xiang^{a, **}, Liping Zhu^a, Mike Tebyetekerwa^{a, b}, Meifang Zhu^{a, *}

^a State Key Laboratory for Modification of Chemical Fibers and Polymer Materials, College of Materials Science and Engineering, Donghua University, Shanghai, 201620, China

^b Research School of Engineering, College of Engineering and Computer Science, The Australian National University, Canberra, Australian Capital Territory, 2601, Australia

ARTICLE INFO

Article history:

Received 10 April 2018

Received in revised form

10 August 2018

Accepted 12 August 2018

Available online 13 August 2018

ABSTRACT

The fabrication of piezoresistive strain sensor with unified and balanced properties of high sensitivity, stretchability, and durability still remains a great challenge due to the oversimplified thin film structure of strain sensor. In this work, a high-performance strain sensor based on conductive poly(styrene-butadiene-styrene)/carbon nanotube fiber (SBS/CNT fiber, SCF) was prepared via wet-spinning. Then, the morphology, mechanical property, piezoresistive performance and sensing mechanism of the SCF-based sensors were systematically investigated. The resultant SCF-based sensors simultaneously demonstrated superior sensitivity (with a gauge factor of 175 under 50% deformation), wide workable range (>260%) and excellent durability due to the excellent flexibility of SBS polymer (the breaking elongation of pure SBS fiber > 1300%), high conductivity of CNT (10^5 S/cm) and the strong π - π interaction between CNT and SBS. These properties make the composite fiber a perfect fit to monitor various large deformation in a wide range of applications. Moreover, the associated sensing mechanism was also systematically explained by tunneling theory and the evolution of the conductive network during the stretching-releasing process.

© 2018 Elsevier Ltd. All rights reserved.

1. Introduction

With the development and continuous requirements of human health monitoring, smart wearable electronics and soft robotics, stretchable strain sensors have drawn a lot of attention in the recent past [1–3]. According to the theoretical and practical requirements, a desirable strain sensor should simultaneously possess high sensitivity, stretchability and stability [4,5]. Obviously, the traditional metal- and semiconductor-based strain sensors cannot fulfil the requirements of stretchable strain sensors due to their flimsiness and poor stretchable properties [6–8]. Therefore, numerous strategies have been proposed to prepare stretchable strain sensors by blending different flexible polymer matrixes (silicone-based elastomers [9–12], rubber [13], thermoplastic

elastomers [14,15]) with conductive nanofillers (carbon materials [16–18], nanowires [19–21], conductive polymers [22–24]) through various processing methods (filtration [25–27], printing [28], transfer [29], coating [30], spray [31], chemical vapor deposition (CVD) [32,33]).

Unfortunately, almost all of the previously reported works were not able to realize conductive polymer-based strain sensors with high stretchability, sensitivity and durability, simultaneously. This is because most of these strain sensors consist of flexible polymers with conductive films, but the features of superior sensitivity (remarkable deformation during loading) and high stretchability (intact morphology during extension) cannot be concurrently obtained through oversimplified thin film structure [2]. For example, Gong et al. reported a highly stretchable sensor composed of the ultrathin gold nanowire and various elastic substrates using drop casting, which could be stretched to 350%, but the *GF* (the gauge factor, *GF*) was less than 9.9 [19]. Also, Yan et al. designed a strain sensor based on polydimethylsiloxane (PDMS)/crumpled graphene/nanocellulose fibril thin film via vacuum filtration, which

* Corresponding author.

** Corresponding author.

E-mail addresses: hengxuexiang@dhu.edu.cn (H. Xiang), zhumf@dhu.edu.cn (M. Zhu).

possessed a wide workable range (>100%) but poor sensitivity ($GF < 8$) [25]. In the same line, Morteza et al. also fabricated stretchable strain sensor based on silicone rubber (Ecoflex)/CNT thin film via air-spray coating and casting. The sensor exhibited high stretchability (>500%) but low sensitivity ($GF < 2.5$) [31]. On the contrary, the highly sensitive strain sensors have been reported using carbon nanomaterials, nanowires, or hybrid nanofillers, which showed high sensitivity ($GF > 1000$) but limited sensing range (<10%) [21,26,32]. Besides, the dynamic durability of the strain sensor is also essential for the practical application of complex deformation needs. In many reports, the degradation of sensing performance has been ascribed to the fatigue deformation of polymer substrates, the fracture of conductive nanomaterials and weak interaction between substrates and nanofillers [2,7].

According to the reported literature, the 1-D conductive nanofillers (e.g. carbon nanotube, CNT) based strain sensors show better stretchability and sensitivity than other nanomaterials owing to the high aspect ratio, excellent elastic performance and ultrahigh piezoresistivity [2]. On the other hand, the SBS is widely employed in strain sensors (as a flexible polymer matrix) due to its superior stretchability, elastic recovery, and processability [34–36]. Moreover, the strong interfacial π - π interaction between CNT and SBS is beneficial to improving the sensitivity and durability of the sensor [16]. Furthermore, the widespread application of the strain sensor is limited by the disadvantages of traditional fabrication methods, which generally are time-consuming, unstable quality, high cost. Fortunately, wet-spinning is a facile and scalable approach to prepare flexible polymer-based strain sensor. And with the fact that 1-D fiber-shaped sensors exhibit greater promise than that of a thin film for practical application, which can be woven into the ordinary clothes or attached to uneven surfaces (e. g. skin), this makes wet-spinning an ideal fabrication process [1,4].

Therefore, the multi-walled carbon nanotube (CNT) and poly(styrene-butadiene-styrene) (SBS) were selected as the conductive nanofiller and flexible polymer matrix to fabricate high sensitive, stretchable and stable strain sensors via a facile and scalable wet-spinning. The effects of CNT content on morphology, percolation threshold and tensile strength were first investigated to ascertain the optimal addition amount of CNT. Subsequently, the hysteresis effect and piezoresistive performance of strain sensors were systematically analyzed using stretching-releasing cycle tests under different applied strains and strain rates. Finally, the theoretical model derived from tunneling theory and the evolution of the conductive network during the loading-unloading process were further researched to understand the sensing mechanism better.

2. Experimental section

2.1. Materials

Poly(styrene-butadiene-styrene) (SBS, D1102K, density 0.94 g/cm³, weight ratio of butadiene/styrene 72/28) was supplied by Kraton, USA. Carbon nanotube (CNT, NC7000, diameter 9.5 nm, length 1.5 μ m, conductivity 10⁵ S/cm) was purchased from Nanocyl, Belgium. Other reagents were supplied by Sinopharm Chemical Reagent Co. Ltd. (Shanghai, China) and used as received without further purification.

2.2. Fabrication of conductive SBS/CNT fibers

The schematic illustration of the preparation process of SBS/CNT fiber (SCF) is shown and proceeded as per Fig. 1 [36]. First, the calculated CNT was dispersed in tetrahydrofuran (THF, 20 ml) with the assistance of ultrasonication at 20 °C for 4 h (S-450D-1/2, Branson, USA) to obtain CNT/THF suspension. Subsequently, the

specific amount of SBS was dissolved in suspension under stirring at room temperature for 24 h. The total weight percent of CNT and SBS was kept at 15 wt. %. Finally, the solution was injected into an ethanol bath to fabricate the conductive SCF through the wet-spinning process. The resultant fibers were denoted as SBS/xCNT, where x represented the weight percent of CNT.

2.3. Characterizations

The morphology of CNT and its dispersity in polymer matrix were characterized by Field emission transmission electron microscope (FE-TEM, JEM-2100F, JEOL, Japan) and field emission scanning electron microscope (FE-SEM, S-4800, Hitachi, Japan). The conductivities of SBS/CNT fibers (SCFs) were investigated using a digital multimeter (Keithley 2000, Tektronix) and high-resistance instrument (PC86, Shanghai Precision and Scientific Instrument Co., Ltd). The specific conductivity (σ) was calculated using equation (1) (Eq. (1)) [37,38], where σ is specific conductivity in S per meter over a gram per cubic centimeter, G is conductance (S), L is length (meter), and LD is linear density (tex), respectively. The tensile strength measurements of SCFs were carried out on a universal testing machine (Instron 5996) at a strain rate of 20 mm/min, and the corresponding results were collected from at least five tests. The mechanical hysteresis effects of SCFs were investigated using cyclic stretching-releasing tests under the applied strain of 50–600% at a strain rate of 20 mm/min. The piezoresistive responses of SCFs were measured using a universal testing machine (Instron 5996) coupled with a Keithley 6487 digital multimeter (Fig. S1). Precisely, two copper electrodes were placed at two ends of SCFs, which were bonded with silver paste to ensure good contact between electrodes and SCFs. The effects of CNT loading on strain sensing performances (sensitivity and stability) were characterized using the periodic extension-retraction tests at different strain rates and strain ranges. The lengths of SCFs in mechanical property and piezoresistive response measurements were 10 mm.

$$\sigma = \frac{G \cdot L}{LD} \times 10^9 \quad (1)$$

3. Results and discussions

3.1. Morphology

The morphology of CNT and its dispersity in SBS matrix were investigated by FE-TEM and FE-SEM. As shown in Fig. S2, the native CNT was multi-walled, crimped, and intertwined with a diameter of 9.5 nm and length of 1.5 μ m, some defects were induced by the ultrasonication step. Fig. 2 exhibited that the cross-sectional morphologies of SBS/CNT fibers (SCFs) were appanate due to the different transfer rates between solvent and coagulation bath [36]. Besides, the CNT was dispersed into SBS matrix in the form of the cluster with slight agglomeration.

3.2. Electrical conductivity

It has been demonstrated that strain sensors near the percolation threshold are highly sensitive but unstable due to the sparse and vulnerable conductive networks. Thus, the weight percentage of conductive nanofillers should be slightly higher than the percolation threshold to balance the sensitivity and stability [9]. Therefore, the percolation threshold of SBS/CNT fiber (SCF) was first characterized before tensile and electromechanical tests to ascertain the optimal addition volume of CNT. As shown in Fig. 3, the

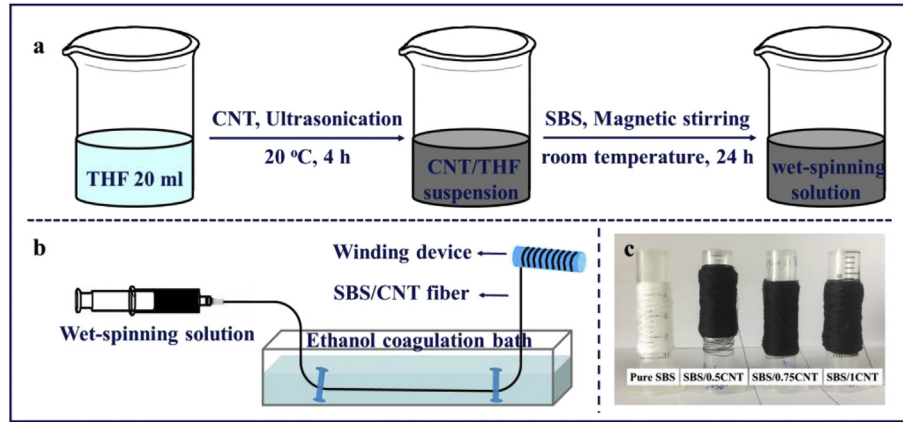


Fig. 1. Schematic illustration of the fabrication process for SBS/CNT fibers (SCFs). (a) Wet-spinning solution preparation, (b) Wet-spinning process, (c) Digital photograph of SCFs with the different weight percent of CNT. (A colour version of this figure can be viewed online.)

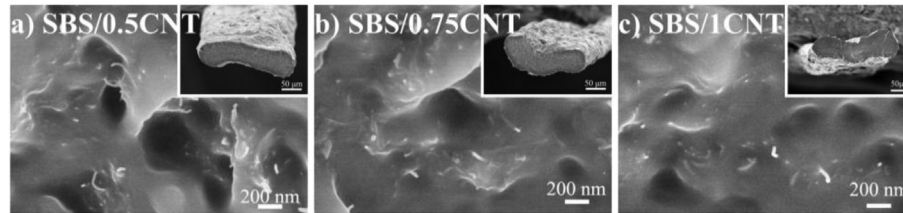


Fig. 2. The cross-sectional FE-SEM images of SBS/CNT fibers.

specific conductivities of SCFs rapidly increased from 10^{-6} to 10^{-2} S/m/g/cm⁻³ as the loading content of CNT increased from 0.25 to 0.40 wt. %, which suggested the continued construction of conducting networks within the fiber. The percolation threshold of SCF was further estimated to be 0.30 wt. % with the help of Eq. (2) and Eq. (3) based on the classical percolation theory [14]:

$$\sigma = \sigma_0 \times (P - P_c)^t \quad (2)$$

$$\log \sigma = \log \sigma_0 + t \times \log(P - P_c) \quad (3)$$

where σ is the fiber conductivity, σ_0 is the scaling factor, P is the weight percentage of CNT, P_c is the percolation threshold, t is the critical exponent. According to the above analysis, the SBS/0.5CNT, SBS/0.75CNT and SBS/1CNT fibers were selected for the further

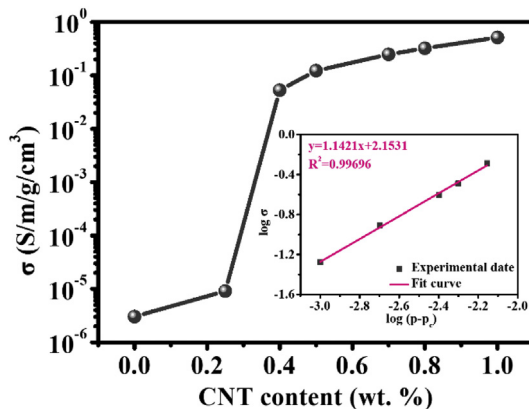


Fig. 3. The effect of CNT content on the specific conductivities of SCFs. (A colour version of this figure can be viewed online.)

mechanical and electromechanical investigations.

3.3. Mechanical property

It is well known that high tensile strength and breaking elongation of the strain sensor are essential for practical applications. Fig. 4 shows that the tensile strengths and elongations at break of SCFs decrease with the increasing CNT loading because of the agglomeration behavior. Fortunately, the breaking elongations of SCFs are higher than 900%, indicating that all SCFs are suitable for fabricating stretchable strain sensor.

It was reported that the mechanical hysteresis of conductive fiber was critical to the stability of the sensor [34]. To better understand the relationship between the viscoelastic behavior of polymer matrix and the reproducibility of the sensor, the hysteresis effect of SCF-based strain sensor was investigated using cyclic loading-unloading tests under the applied strain ranging from 50 to 600% at the strain rate of 20 mm/min. For example, the stress-strain curves of the SBS/1CNT fiber under different applied strains were shown in Fig. 5a. Apparently, the releasing curves were inconsistent with the stretching curves in each cycle, implying the mechanical hysteresis existed in SCFs during cyclic extension-retraction test due to the irreversible slip of SBS molecular chain [35]. The elastic recoveries (ER_e) of SCFs were further calculated using Eq. (4) [39]:

$$ER_e = \frac{(\varepsilon - \varepsilon_R)}{\varepsilon} \times 100\% \quad (4)$$

where ε and ε_R are the applied strain and residual strain, respectively. Fig. 5b demonstrated that the elastic recovery increased with increasing applied strain but gradually decreased with increasing CNT loading. It's noted that all the elastic recoveries were higher than 85%, which can fulfil the requirement of the practical application.

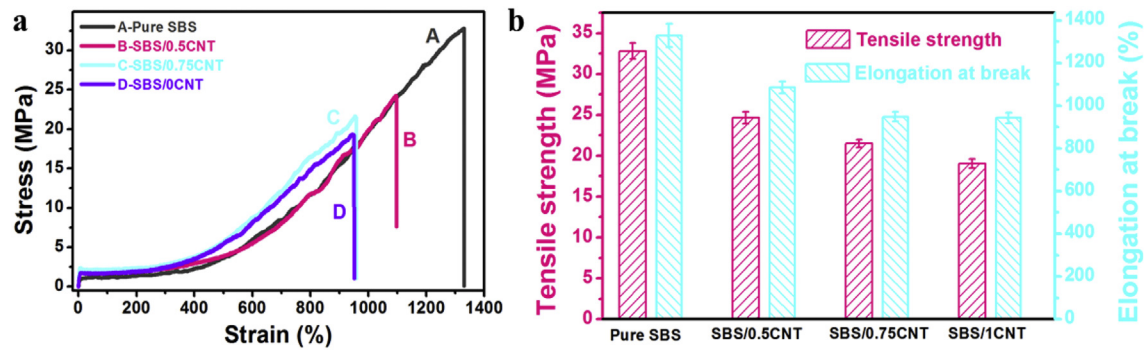


Fig. 4. Mechanical property of SCFs. (a) Stress-strain curves, (b) Comparison of mechanical properties. (A colour version of this figure can be viewed online.)

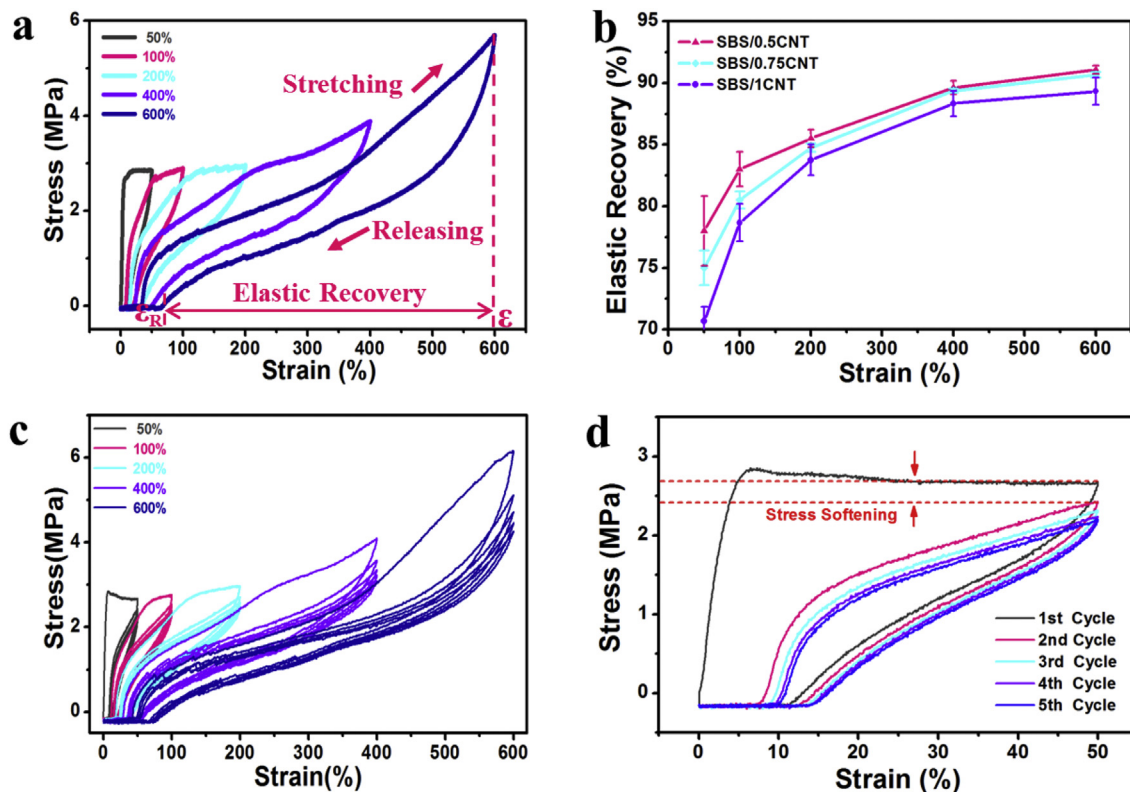


Fig. 5. Mechanical hysteresis effect of SCFs. (a) Stress-strain curves of SBS/1CNT fiber for single cyclic test under 50–600% applied strain, (b) Elastic recoveries of SCFs during stretching-releasing test, (c) Mechanical hysteresis of SBS/1CNT fiber for five cycles under the 50–600% deformation at the strain rate of 20 mm/min, (d) Stress softening of SBS/1CNT fiber for five cycles under 50% applied strain. (A colour version of this figure can be viewed online.)

The effects of applied strain and cycle times on mechanical hysteresis were further investigated using loading-unloading tests for 5 cycles under 50–600% applied strain at the strain rate of 20 mm/min. As shown in Fig. 5c, the mechanical hysteresis was observed under different strains, which increased with the increasing applied strain due to the physical breakage and rearrangement of SBS molecular chains during stretching-releasing test [34–36]. It was reported that CNT/polymer composites based strain sensors usually showed a linear response under low strains ($\epsilon < 1\%$), but followed by non-linearity at larger strains. As a rule, once the microstructure of strain sensor undergoes change from “homogeneous morphology” to “nonhomogeneous morphology” upon stretching, strain sensors respond to the mechanical property with a nonlinear manner. Furthermore, change of the “homogeneous percolation network” to the “inhomogeneous percolation network”

for the low-density CNT network sensor was found as the main reason of nonlinearity [2,40]. Besides, Fig. 5d revealed that the stress-softening (mechanical hysteresis) for SBS/1CNT under 50% applied strain exhibited the most drastic change in the first cycle and immediately trended toward a constant value. According to the reported literature, the irreversible destruction of the polymer matrix mainly occurs in the initial cycle, then the following cycles need less power to reach the same deformation [36].

3.4. Piezoresistive performance

The effect of CNT loading on the piezoresistive behavior was evaluated by plotting relative resistance changes ($\Delta R/R_0$, where $\Delta R = R - R_0$, R is instantaneous resistance, R_0 is initial resistance) as a function of applied strain. As shown in Fig. S3 and 6a, the ($\Delta R/R_0$)

increased rapidly with the increasing deformation and CNT loading under the same experimental conditions. According to the Simmons theory, the average distances between two adjacent CNTs increase during the extension process. Thus some conductive pathways in the polymer matrix are destroyed and the resistance exponentially increases with applied strain [2].

The piezoresistive sensitivity was further investigated using gauge factor (GF , $GF = (\Delta R/R_0)/\epsilon$) [10], the curves of GF -strain were provided in Fig. 6b. It was observed that the GF values of different SCFs were almost the same when the applied strain was lower than 10%, which can be easy to comprehend that the distances of adjacent CNTs were shorter than critical tunneling distance and the conductive network still could keep the fine and stable state under small deformation [26]. However, the GF values significantly increased with the increasing CNT loading when the applied strain was higher than 10%, which was closely related to the different dispersed states of CNT in SBS matrix [16,41]. For SBS/1CNT fiber, the CNT was dispersed in the form of cluster with some agglomeration and the reduction of the conductive network was sharp under large deformation, which led to the sudden variation in electrical resistance during stretching. Compared with the SBS/1CNT, the dispersity of CNT in SBS/0.5CNT was more homogeneous with less agglomeration, thus the breakdown of conductive pathway was more gradual without sharp change during the extension process. Besides, the GF values of SBS/0.75CNT and SBS/1CNT fibers became enormously high when the applied strain was larger than 267%. In theory, the conductive network in SBS matrix would be heavily destroyed under tremendous deformation when the distances between neighbouring CNTs was higher than critical tunneling space, which resulted in the explosive growth of instantaneous resistance and GF value [8]. The similar phenomenon was also found in the SBS/0.5CNT fiber, but its critical applied strain

(87%) was much smaller than those of SBS/0.75CNT and SBS/1CNT fibers (267%) due to the lower CNT content and sparser conductive network in the polymer matrix. Furthermore, the most substantial working ranges of SBS/0.5CNT, SBS/0.75CNT and SBS/1CNT fibers are 87%, 267%, and 267%, respectively. The corresponding GF values of SCFs under the maximum workable applied strain are 28, 375, and 2889, respectively. Therefore, the SCFs (especially the SBS/1CNT fiber) based sensors simultaneously possess an excellent sensitivity and stretchability, which are superior to the recently reported sensors (Fig. 6c and Table S1). Furthermore, the response time of the SCF-based sensor was further determined to be less than 107 ms, which was evaluated by a quasi-time step strain (Fig. S4).

The dynamic reliability and durability of SCFs-based sensors were confirmed using stretching-releasing cyclic test under 50% applied strain at a strain rate of 5 mm/min. As shown in Fig. 7a, the $(\Delta R/R_0)$ s of SCFs showed the periodic fluctuation during the cyclic test, which was caused by the destruction and reconstruction of conductive networks due to the variation of distance between conductive CNTs during loading-unloading cycles [9]. It was found that the final $(\Delta R/R_0)$ value after unloading was much higher than the initial one in the first cycle, indicating that some conductive networks were permanently destroyed in stretching process owing to the irreversible slip of SBS molecular chain (called electromechanical hysteresis) [34]. Satisfyingly, the $(\Delta R/R_0)$ exhibited good repeatability without hysteresis effect and “shoulder peak” phenomenon after the first cycle, which was similar to the mechanical hysteresis [18,28]. Besides, the $\Delta R/R_0$ response of strain sensor based on SBS/1CNT fiber further exhibited excellent stability during 200 stretching-releasing cycles except for the overshoot of incipient cycles due to the viscoelastic nature of SBS matrix (Fig. S5).

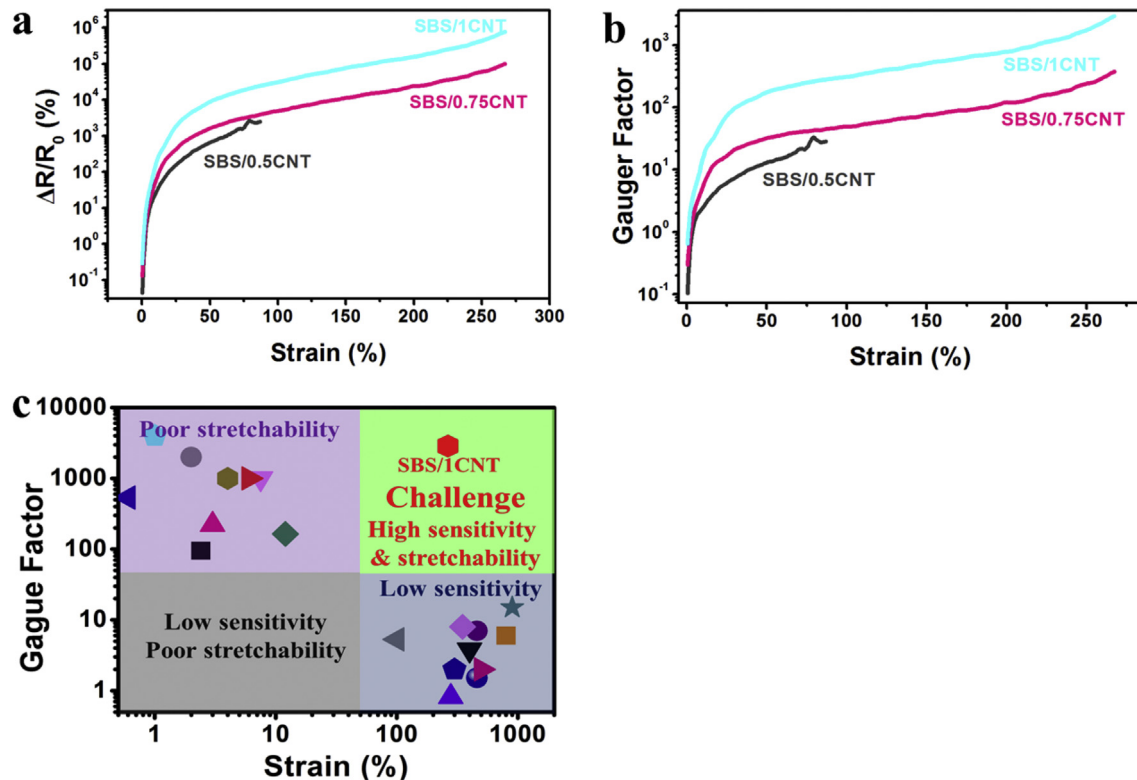


Fig. 6. Piezoresistive performance of SCFs. (a) $\Delta R/R_0$ and (b) GF of SCFs as a function of applied strain ($\Delta R/R_0$ and GF axes are in Log), (c) Comparison of GF and maximum workable range of SBS/1CNT fiber-based sensor with those of recently reported piezoresistive strain sensors (See Table S1). (A colour version of this figure can be viewed online.)

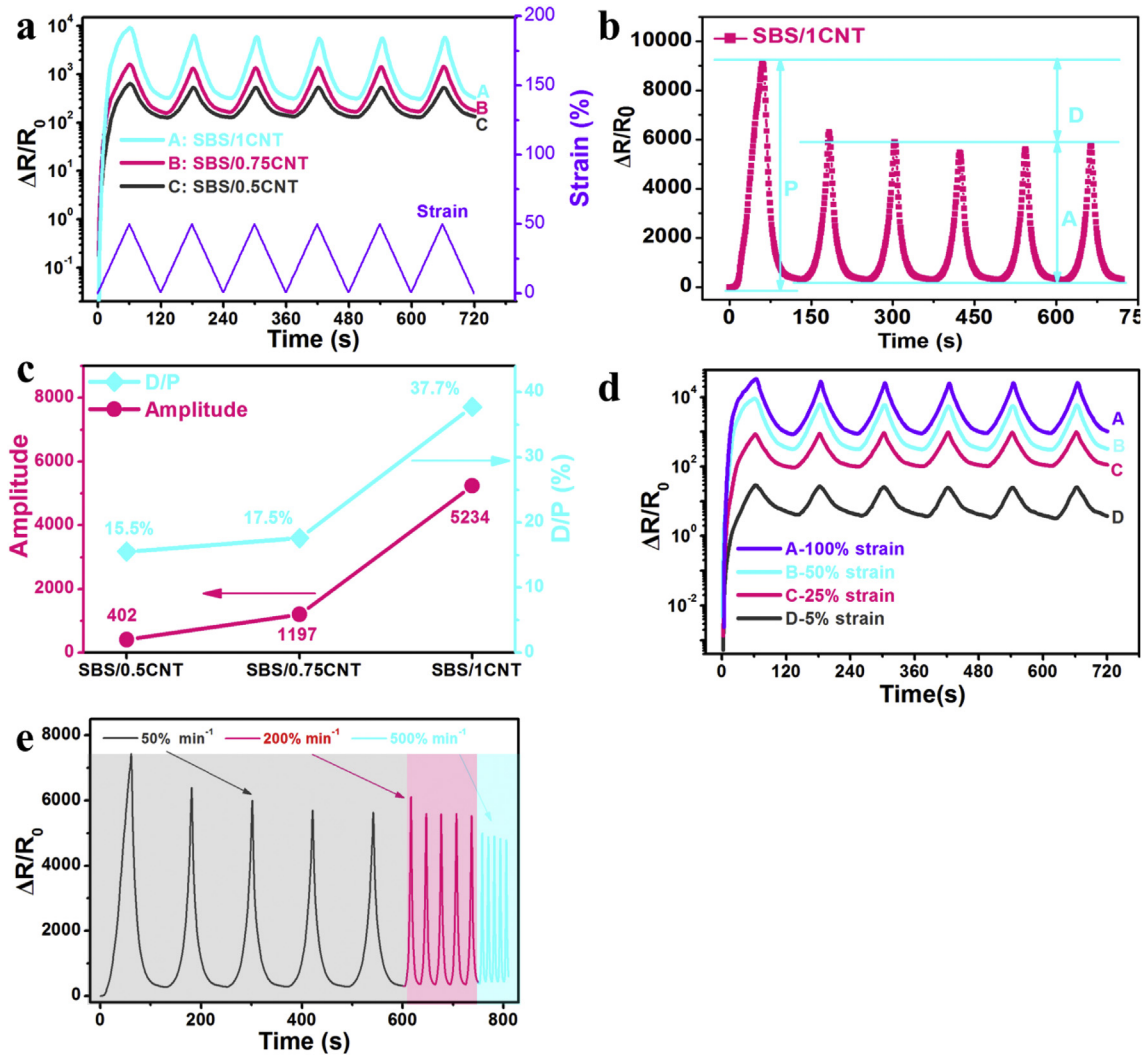


Fig. 7. Dynamic reliability and durability of SCFs. (a) $\Delta R/R_0$ of SCFs as a function of time ($\Delta R/R_0$ axes are in Log), (b) The implication of attenuation degree of sensitivity (D/P) and averaged amplitude of $\Delta R/R_0$ after the first cycle (A), (c) The D/P and A of SCFs, effects of strain amplitude (d) and strain rate (e) on the dynamic sensing performance of SBS/1CNT. (A colour version of this figure can be viewed online.)

The attenuation degree of sensitivity (defined as the ratio of D/P , D is the variation of peak $\Delta R/R_0$, P is the maximum $\Delta R/R_0$ in the first cycle) and averaged amplitude of $\Delta R/R_0$ after the first cycle (A) were further investigated to better evaluate the dynamic reliability and durability. The lower D/P and higher A suggest the better reproducibility and sensibility, respectively [16]. As shown in Fig. 7b and c, the D/P and A increased with CNT loading, demonstrating that the sensor with higher CNT content was more sensitive but less stable due to different dispersed states of CNT and structures of conductive networks in SBS matrix, which has been well explained in Fig. 6b.

The SBS/1CNT fiber was selected to further analyze the effects of applied strain and strain rate on piezoresistive performance. As shown in Fig. 7d, the ($\Delta R/R_0$) of SBS/1CNT fiber increased with the increasing applied strain and immediately reached a steady state after the first cycle under different applied strains, while the reported sensors have to be stretched and released for several even dozens of cycles before achieving the stable ($\Delta R/R_0$) [17,18,24,42]. Therefore, these results confirmed that the SCFs-based sensor exhibited better reproducibility and durability than the reported works, which can be attributed to excellent elastic performances of

SBS and CNT, the strong π - π interaction between SBS and CNT.

The dynamic stability of SBS/1CNT fiber was further investigated under 50% applied strain at the different strain rates. As shown in Fig. 7e, the constant ($\Delta R/R_0$) values of SBS/1CNT fiber were almost the same with a slight variation at the strain rate of 5, 20, and 50 mm/min, demonstrating that the reliability of SBS/CNT sensors had a negligible dependency on strain rate. It was noted that the ($\Delta R/R_0$) value showed a noticeable reduction at the strain rate of 50 mm/min owing to the mismatch between strain rate and multimeter. In conclusion, the results of piezoresistive performance confirmed that the SCF-based sensors concurrently exhibited excellent sensitivity, stretchability and durability, which showed great promise for practical application.

3.5. Strain sensing mechanism

Generally speaking, the strain sensing mechanism of flexible polymer-based sensor depends on the tunneling effect [2]. The modelling analysis of strain sensing behaviors at different applied strains was further explored using a theoretical model [16,36,42]. Thus the resistance can be expressed by Eqs. (5) and (6):

$$R = \left(\frac{L}{N}\right) \times \left(\frac{8\pi hs}{3\gamma a^2 e^2}\right) \times \exp(\gamma s) \quad (5)$$

$$\gamma = \frac{4\pi\sqrt{2m\lambda}}{h} \quad (6)$$

where R is the resistance, L is the number of CNTs in a single conductive pathway, N is the quantity of conducting paths, h is Plank's constant, s is the least distance between CNTs, a^2 is the effective sectional area, e is the electron charge, m is the electron mass, λ is the height of the potential barrier between the adjacent CNTs. It is well known that the tunneling resistance increases with the increasing distances between nanofillers during extension. Thus the average distances of CNTs increase from s_0 to s , and the number of conductive pathways decreases from N_0 to N , the relationship between s , N and ε (applied strain) can be calculated by Eqs. (7) and (8):

$$s = s_0(1 + b\varepsilon) \quad (7)$$

$$N = \frac{N_0}{\exp(A\varepsilon + B\varepsilon^2 + C\varepsilon^3 + D\varepsilon^4)} \quad (8)$$

Where b , A , B , C , and D are constants. Finally, $(\Delta R/R_0)$ is given as follows Eq. (9):

$$\frac{\Delta R}{R} = (1 + b\varepsilon) \times \exp\left[(A + \gamma bs_0)\varepsilon + B\varepsilon^2 + C\varepsilon^3 + D\varepsilon^4\right] - 1 \quad (9)$$

As shown in Fig. 8, the imitation coefficient of tunneling effect for strain sensing behavior is quite good ($R^2 = 0.99973$), implying that the strain sensing mechanism can be well explained by the tunneling effect.

The schematic diagram for the evolution of the conductive network during the extension-retraction test was presented to explain the mechanism better. According to the tunneling effect, the tunneling resistance can be approximately calculated according to Eq. (10) [26], and the critical distance of two adjacent CNTs is about 1–1.8 nm [2].

$$R_{\text{tunnel}} = \frac{V}{A \times J} = \frac{h^2 d}{Ae^2 \sqrt{2m\lambda}} \exp\left(\frac{4\pi d}{h} \sqrt{2m\lambda}\right) \quad (10)$$

Where V is the potential difference, A is the sectional area of the

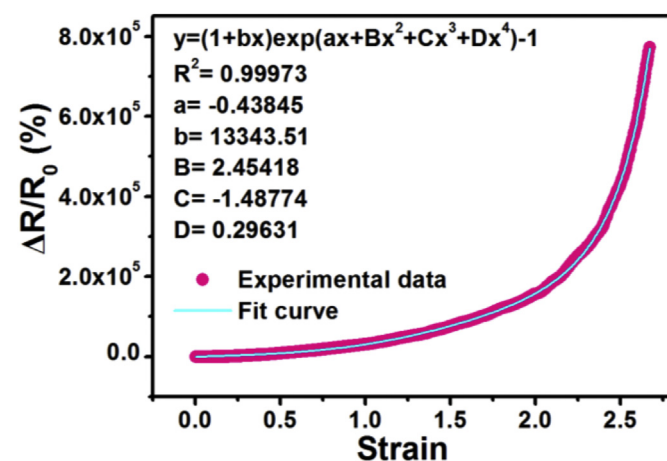


Fig. 8. Experimental (pink dots) and theoretical (solid blue line) data of $\Delta R/R_0$ as a function of strain. (A colour version of this figure can be viewed online.)

tunnel, J is the density of tunneling current, h is Plank's constant, d is the distance between CNTs, e is the electron charge, m is the electron mass, λ is the height of the potential barrier between the adjacent CNTs. The electron can travel through the polymer and generate tunneling current when the distance between two adjacent CNTs is shorter than the critical distance [42]. Otherwise, the conductive network is gravely destroyed, and the tunneling resistance is regarded to exist up to infinity. As shown in Fig. 9, the conductive network of SCF is the most compact, and the resistance is minimum before extension due to the least average distance between two adjacent CNTs during cyclic the test. The $(\Delta R/R_0)$ of SCF-based strain sensor will periodically change with applied strain due to the destruction and reconstruction of conductive networks in the cycling test, which is caused by the periodic change of distance between adjoining CNTs. During the stretching phase, the distance between two adjacent CNTs increases with the increasing applied strain. Thus the destruction of the conductive network prevails, and the $(\Delta R/R_0)$ of the SCF-based strain sensor significantly increases with strain. During the releasing phase, the space between two adjacent CNTs decreases with the decreasing applied strain. Hence, the reconstruction of the conductive network is predominant, and the $(\Delta R/R_0)$ of SCF based strain sensor sharply decreases with deformation.

4. Conclusion

In this study, the highly sensitive and stretchable strain sensor based on conductive SBS/CNT fiber (SCF) was prepared via wet-spinning. The morphology, mechanical property, piezoresistive performance and sensing mechanism of the SCF-based sensor were systematically investigated. The SEM images exhibited that CNT was distributed in SBS polymer matrix in the form of cluster with some agglomeration. Besides, the CNT dispersed state and conductive network in the SBS matrix were vitally affected by CNT content. Thus the sensitivity and durability of the strain sensor could be controlled by changing CNT loading. From the test results, the strain sensor with higher CNT loading exhibited better sensitivity but worse durability during the dynamic stretching-releasing tests. However, the piezoresistive performance of the SCF-based sensor was superior to many previously reported sensors, especially the SBS/1CNT fiber possessed the maximum workable strain range of 267% and the highest GF value of 2889. Furthermore, most of the hysteresis effect, caused by the irreversible slip of SBS molecular chain, mainly occurred in the first cycle, then the sensors showed utterly repeatable sensitivity without hysteresis effect and

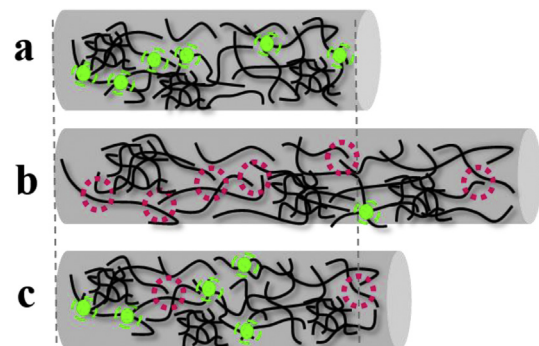


Fig. 9. Schematic diagram for the evolution of conductive network in SCFs during the stretching-releasing cyclic test. (Note: a. Initial state, b. Stretched state, c. Released state. Red and green dotted lines represent the destruction and reconstruction of the conductive network during stretched and released state, respectively.) (A colour version of this figure can be viewed online.)

“shoulder peak” phenomenon after the first cycle, suggesting that SCF strain sensors had an excellent dynamic reproducibility and durability. Moreover, the theoretical model derived from tunneling theory and the evolution of conductive polymer network during loading-unloading processes were further investigated to better understand the sensing mechanism. The results exhibited that the theoretical model coincided well with the experimental data and that the sensing performance significantly depended on the distance between the adjacent CNTs during the cyclic tests. Such reported stretchable 1-D composite piezoresistive strain fiber with superior sensitivity, excellent flexibility and high conductivity presented in this work can find applications in various biomedical, artificial intelligence, soft robotic and smart wearable applications.

Acknowledgements

This work was supported by the National Natural Science Foundation of China (51733002), the program for Changjiang Scholars and Innovative Research Team in University (IRT16R13), the Fundamental Research Funds for the Central Universities (2232018A3-01, 2232018D3-03), Shanghai Fundamental Research Projects (16JC1400701), the Innovation Program of Shanghai Municipal Education Commission (E00055), and Opening Project of State Key Laboratory of for Modification of Chemical Fibers and Polymer Materials, Donghua University (LK1607).

Appendix A. Supplementary data

Supplementary data related to this article can be found at <https://doi.org/10.1016/j.carbon.2018.08.028>.

References

- [1] W. Zeng, L. Shu, Q. Li, S. Chen, F. Wang, X.M. Tao, Fiber-based wearable electronics: a review of materials, fabrication, devices, and applications, *Adv. Mater.* 26 (31) (2014) 5310–5336.
- [2] M. Amjadi, K. Kyung, I. Park, M. Sitti, Stretchable, skin-mountable, and wearable strain sensors and their potential applications: a review, *Adv. Funct. Mater.* 26 (11) (2016) 1678–1698.
- [3] K. Takei, W. Honda, S. Harada, T. Arie, S. Akita, Toward flexible and wearable human-interactive health-monitoring devices, *Adv. Healthcare Mater.* 4 (4) (2014) 487–500.
- [4] Z.H. Tang, S.H. Jia, F. Wang, C.S. Bian, Y.Y. Chen, Y.L. Wang, et al., Highly stretchable core-sheath fibers via wet-spinning for wearable strain sensors, *ACS Appl. Mater. Interfaces* 10 (7) (2018) 6624–6635.
- [5] S.F. Zhao, J.H. Li, D.X. Cao, G.P. Zhang, J. Li, K. Li, et al., Recent advancements in flexible and stretchable electrodes for electromechanical sensors: strategies, materials, and features, *ACS Appl. Mater. Interfaces* 9 (14) (2017) 12147–12164.
- [6] H. Marek, N. Daniel, K. Jing, H. Mario, A novel class of strain gauges based on layered percolative films of 2D materials, *Nano Lett.* 12 (11) (2012) 5714–5718.
- [7] M. Amjadi, A. Pichitpajongkit, S. Lee, S. Ryu, I. Park, Highly stretchable and sensitive strain sensor based on silver nanowire-elastomer nanocomposite, *ACS Nano* 8 (5) (2014) 5154–5163.
- [8] C.X. Liu, J.W. Choi, Analyzing resistance response of embedded PDMS and carbon nanotubes composite under tensile strain, *Microelectron. Eng.* 117 (1) (2014) 1–7.
- [9] M. Wang, K. Zhang, X.X. Dai, Y. Li, J. Guo, H. Liu, et al., Enhanced electrical conductivity and piezoresistive sensing in multi-wall carbon nanotubes/polydimethylsiloxane nanocomposites via the construction of a self-segregated structure, *Nanoscale* 9 (31) (2017) 11017–11026.
- [10] X. Wang, J.F. Li, H.N. Song, H.L. Huang, J.H. Gou, Highly stretchable and wearable strain sensor based on printable carbon nanotube layers/polydimethylsiloxane composites with adjustable sensitivity, *ACS Appl. Mater. Interfaces* 10 (8) (2018) 7371–7380.
- [11] S.J. Park, J. Kim, M. Chu, M. Khine, Highly flexible wrinkled carbon nanotube thin film strain sensor to monitor human movement, *Adv. Mater. Technol.* 1 (5) (2016) 1600053–1600060.
- [12] S.H. Bae, Y. Lee, B.K. Sharma, H.J. Lee, J.H. Kim, J.H. Ahn, Graphene-based transparent strain sensor, *Carbon* 51 (2013) 236–242.
- [13] S. Tadakaluru, W. Thongsuwan, P. Singjai, Stretchable and flexible high-strain sensors made using carbon nanotubes and graphite films on natural rubber, *Sensors* 14 (1) (2014) 868–876.
- [14] C. Hu, Z.Y. Li, Y.L. Wang, J.C. Gao, K. Dai, G.Q. Zheng, et al., Comparative assessment of the strain-sensing behaviors of polylactic acid nanocomposites: reduced graphene oxide or carbon nanotubes, *J. Mater. Chem. C* 5 (9) (2017) 2318–2328.
- [15] H. Tian, Y. Shu, Y.L. Cui, W.T. Mi, Y. Yang, D. Xie, et al., Scalable fabrication of high-performance and flexible graphene strain sensors, *Nanoscale* 6 (2) (2014) 699–705.
- [16] L.Y. Duan, S.R. Fu, H. Deng, Q. Zhang, K. Wang, F. Chen, et al., The resistivity-strain behavior of conductive polymer composites: stability and sensitivity, *J. Mater. Chem. A* 2 (40) (2014) 17085–17098.
- [17] J.D. Shi, J. Hu, Z.H. Dai, W. Zhao, P. Liu, L.Y. Zhao, et al., Graphene welded carbon nanotube crossbars for biaxial strain sensors, *Carbon* 123 (2017) 786–793.
- [18] P. Costa, J. Nunes-Pereira, J. Oliveira, J. Silva, J.A. Moreira, S.A.C. Carabineiro, et al., High-performance graphene-based carbon nanofiller/polymer composites for piezoresistive sensor applications, *Compos. Sci. Technol.* 153 (2017) 241–252.
- [19] S. Gong, D.T.H. Lai, B. Su, K.J. Si, Z. Ma, L.W. Yap, et al., Highly stretchy black gold e-skin nanopatches as highly sensitive wearable biomedical sensors, *Adv. Electron. Mater.* 1 (4) (2015) 1400063–1400069.
- [20] G.H. Lim, N.E. Lee, B. Lim, Highly sensitive, tunable, and durable gold nano-sheet strain sensors for human motion detection, *J. Mater. Chem. C* 4 (24) (2016) 5642–5647.
- [21] D. Kang, P.V. Pikhitsa, Y.W. Choi, C. Lee, S.S. Shin, L.F. Piao, et al., Ultrasensitive mechanical crack-based sensor inspired by the spider sensory system, *Nature* 516 (7530) (2014) 222–226.
- [22] M.F. Li, H.Y. Li, W.B. Zhong, Q.H. Zhao, D. Wang, Stretchable conductive polypyrrole/polyurethane (PPy/PU) strain sensor with netlike microcracks for human breath detection, *ACS Appl. Mater. Interfaces* 6 (2) (2014) 1313–1319.
- [23] E. Roh, B.U. Hwang, D. Kim, B.Y. Kim, N.E. Lee, Stretchable, transparent, ultrasensitive, and patchable strain sensor for human-machine interfaces comprising a nanohybrid of carbon nanotubes and conductive elastomers, *ACS Nano* 9 (6) (2015) 6252–6261.
- [24] J. Teixeira, L. Horta-Romaris, M.J. Abad, P. Costa, S. Lanceros-Mendez, Piezoresistive response of extruded polyaniline/(styrene-butadiene-styrene) polymer blends for force and deformation sensors, *Mater. Des.* 141 (2018) 1–8.
- [25] C.Y. Yan, J.X. Wang, W.B. Kang, M.Q. Cui, X. Wang, C.Y. Foo, et al., Highly stretchable piezoresistive graphene-nanocellulose nanopaper for strain sensors, *Adv. Mater.* 26 (13) (2014) 2022–2027.
- [26] S. Chen, Y. Wei, S.M. Wei, Y. Li, L. Liu, Ultrasensitive cracking-assisted strain sensors based on silver nanowires/graphene hybrid particles, *ACS Appl. Mater. Interfaces* 8 (38) (2016) 25563–25570.
- [27] T. Wang, R.R. Wang, Y. Cheng, J. Sun, Quasi in situ polymerization to fabricate copper nanowire-based stretchable conductor and its applications, *ACS Appl. Mater. Interfaces* 8 (14) (2016) 9297–9304.
- [28] J.F. Christ, N. Aliheidari, A. Ameli, P. Potschke, 3D printed highly elastic strain sensors of multiwalled carbon nanotube/thermoplastic polyurethane nanocomposites, *Mater. Des.* 131 (2017) 394–401.
- [29] P. Lee, J. Ham, J. Lee, S. Hong, S. Han, Y.D. Suh, et al., Highly stretchable or transparent conductor fabrication by a hierarchical multiscale hybrid nanocomposite, *Adv. Funct. Mater.* 24 (36) (2014) 5671–5678.
- [30] M.C. Zhang, C.Y. Wang, Q. Wang, M.Q. Jian, Y.Y. Zhang, Sheath-Core graphite/silk fiber made by dry-meyer-rod-coating for wearable strain sensors, *ACS Appl. Mater. Interfaces* 8 (32) (2016) 20894–20899.
- [31] M. Amjadi, Y.J. Yoon, I. Park, Ultra-stretchable and skin-mountable strain sensors using carbon nanotubes-ecoflex nanocomposites, *Nanotechnology* 26 (37) (2015) 375501–375511.
- [32] X. Li, R.J. Zhang, W.J. Yu, K.L. Wang, J.Q. Wei, D.H. Wu, et al., Stretchable and highly sensitive graphene-on-polymer strain sensors, *Sci. Rep.* 2 (2012) 870–875.
- [33] Y. Wang, L. Wang, T.T. Yang, X. Li, X.B. Zang, M. Zhu, et al., Wearable and highly sensitive graphene strain sensors for human motion monitoring, *Adv. Funct. Mater.* 24 (29) (2014) 4666–4670.
- [34] P. Costa, S. Ribeiro, S. Lanceros-Mendez, Mechanical vs. Electrical hysteresis of carbon nanotube/styrene-butadiene-styrene composites and their influence in the electromechanical response, *Compos. Sci. Technol.* 109 (2015) 1–5.
- [35] P. Costa, S. Silvia, J.C. Viana, S. Lanceros-Mendez, Extruded thermoplastic elastomers styrene-butadiene-styrene/carbon nanotubes composites for strain sensor applications, *Compos. B Eng.* 57 (2014) 242–249.
- [36] X.P. Wang, S. Meng, T. Mike, Y.L. Li, J. Pionteck, B. Sun, et al., Highly sensitive and stretchable piezoresistive strain sensor based on conductive poly(styrene-butadiene-styrene)/few layer graphene composite fiber, *Compos. Part A-App. S.* 105 (2018) 291–299.
- [37] A. Lekawa-Raus, J. Patmore, L. Kurzepa, J. Bulmer, K. Koziol, Electrical properties of carbon nanotube based fibers and their future use in electrical wiring, *Adv. Funct. Mater.* 24 (24) (2014) 3661–3682.
- [38] A. Lekawa-Raus, L. Kurzepa, X.Y. Peng, K. Koziol, Towards the development of carbon nanotube based wires, *Carbon* 68 (2014) 597–609.
- [39] M.Z. Seyedin, J.M. Razal, P.C. Innis, R. Jalili, G.G. Wallace, Achieving outstanding mechanical performance in reinforced elastomeric composite fibers using large sheets of graphene oxide, *Adv. Funct. Mater.* 25 (1) (2015) 94–104.

- [40] S. Cravanzola, G. Haznedar, D. Scarano, A. Zecchina, F. Cesano, Carbon-based piezoresistive polymer composites: structure and electrical properties, *Carbon* 62 (2013) 270–277.
- [41] S. Gong, Z.H. Zhu, On the mechanism of piezoresistivity of carbon nanotube polymer composites, *Polymer* 55 (16) (2014) 4136–4149.
- [42] H. Liu, Y.L. Li, K. Dai, G.Q. Zheng, C.T. Liu, C.Y. Shen, et al., Electrically conductive thermoplastic elastomer nanocomposites at ultralow graphene loading levels for strain sensor applications, *J. Mater. Chem. C* 4 (1) (2016) 157–166.